Insights into the antiproliferative mechanism of (C^N)-chelated half-sandwich iridium complexes

Robin Ramos,[a,b] Jérémy M. Zimbron,[a] Serge Thorimbert,[a] Lise-Marie Chamoreau,[a] Annie Munier,[b] Candice Botuha,[a] Anthi Karaiskou,[b] Michèle Salmain,*[a] and Joëlle Sobczak-Thépot*[b]

Transition metal-based anticancer compounds, as alternative to platinum derivatives, are raising scientific interest as they may present distinct although poorly understood mechanisms of action. We used a structure-activity relationship-based methodology to investigate the chemical and biological features of a series of ten (C^N)-chelated half-sandwich iridium^{III} complexes of the general formula [IrCp*(phox)Cl], where (phox) is a 2-phenyloxazoline ligand forming a 5-membered metallacycle. This series of compounds undergoes a fast exchange of their chlorido ligand once solubilised in DMSO. They were cytotoxic to HeLa cells with IC_{50} values in the micromolar range and induced a rapid activation of caspase-3, an apoptosis marker. *In vitro*, the oxidative power of all the complexes towards NADH was highlighted but only the complexes bearing substituents on the oxazoline ring were able to produce H_2O_2 at the micromolar range. However, we demonstrated using a powerful HyPer protein redox sensor-based flow cytometry assay that most complexes rapidly raised intracellular levels of H_2O_2. Hence, this study shows that oxidative stress can partly explain the cytotoxicity of these complexes on the HeLa cell line and gives a first entry to their mechanism of action

Introduction

Platinum-based compounds in association with other cytotoxic agents are still among the most frequently prescribed anticancer drugs, despite their severe side effects and resistance developed by many tumours. Alternative metal-based compounds, among which various ruthenium^{II} and ruthenium^{III} complexes,[1] are raising scientific interest as they may present original multi-targeting mechanisms of action (MoA) that stand out from the classical DNA-damage inducers and antimitotics.

Iridium complexes provide other potentially useful alternatives to platinum-based anticancer drugs. In the iridium(III) family, the octahedral, bis-cyclometallated complexes of the general formula $[Ir^{III}(C^N)^2(N^N)]^+$, X^- are well known for their luminescence properties owing to metal-to-ligand charge transfer (MLCT) transitions making them popular imaging probes as well as photodynamic therapy agents.[2,3] The second series, namely the so-called half-sandwich complexes, presents a different coordination pattern with a pseudo-tetrahedral geometry. The iridium centre is coordinated by a penta-substituted cyclopentadienyl ligand (typically pentamethyl cyclopentadienyl, Cp*), a chelating bidentate ligand and often a chlorido ligand occupying the last coordination position. The lability of this last ligand makes the complexes reactive towards various substrates, hence their initial application as hydrogenation and C-H activation catalysts.[4–6]

The antiproliferative properties of half-sandwich complexes bearing a C^N chelating ligand were first reported in 2011.[7] Subsequent reports allowed to delineate the structural parameters (charge, nature of the chelating ligand, degree of lability of the third ligand) governing their cytotoxicity.[8–11] For some complexes, a relationship between cytotoxicity and rapid raise of total intracellular reactive oxygen species (ROS) was highlighted[12] with concomitant upregulation of antioxidant responses.[13] More generally, the ability of molecules to modulate the oxidation stress represents an innovative strategy to preferentially target cancer cells owing to their unique metabolic properties.[14,15]

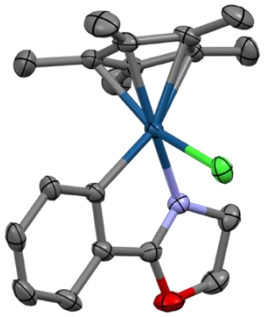

Because the relationship between cytotoxicity, *in vitro* generation of H_2O_2 and intracellular H_2O_2 levels had never been experimentally demonstrated, we undertook to investigate it on a library of half-sandwich iridium(III) complexes. For this purpose, ten complexes **Ir1-10** comprising variously substituted 2-phenyloxazolines (phox) **L1-10** as C^N chelating ligands were synthesized and characterized. The phox scaffold was selected owing to the readiness to introduce a wide range of electron-donating or withdrawing substituents on either of the 2 rings and a second stereogenic centre on the

oxazoline ring. A structure-activity relationship study was systematically performed regarding their antiproliferative properties on the HeLa cell model together with their ability to elicit the production of hydrogen peroxide *in vitro* and *in vivo*. Using a robust and selective flow cytometric approach with the endogenously expressed protein redox sensor HyPer, we showed that some of the complexes induce a fast and long-lasting perturbation of intracellular H_2O_2 levels. This behaviour was correlated to their ability to catalyse the production of H_2O_2 from NADH in aerated physiological environment.

Results and Discussion

Synthesis and characterization

The synthetic route to the ten half-sandwich complexes **Ir1-10** with the general structure [Cp*(C^N)IrCl] is reported in Scheme 1. The substitution patterns aimed at examining the influence of steric effects and stereochemistry ($R^{2,3}$) as well as electronic effects (R^1) on the chemical and biological properties of the complexes.

Ligand **L1** is commercially available and compounds **L2-10** were obtained in two or three steps in moderate to high yields. The condensation of ß-ethanolamines with para-substituted benzoyl chlorides was followed by an oxidation step using excess $SOCl_2$. For **L5** and **L6** this led to a simple chlorination of the N-(2-hydroxyethyl) benzamide intermediate. Hence, another step was required and NaH was employed to induce cyclization from the nitrogen's lone pair (Procedure B). Global yields for the synthesis of **L2-10** were comprised between 40-99%. Following procedures from the previously reported structures **Ir1**,[16] **Ir2**[17] and **Ir8**[18], sodium acetate was used to produce **Ir1-10** from $[Cp^*IrCl_2]_2$ with the corresponding (phox) ligands (**L1-10)** in moderate to good yields (38-97%).

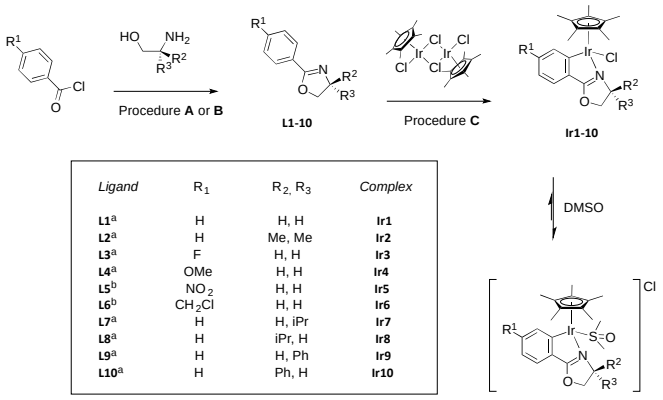

Ligand	R_1	R_2, R_3	*Complex*
L1[a]	H	H, H	**Ir1**
L2[a]	H	Me, Me	**Ir2**
L3[a]	F	H, H	**Ir3**
L4[a]	OMe	H, H	**Ir4**
L5[b]	NO_2	H, H	**Ir5**
L6[b]	CH_2Cl	H, H	**Ir6**
L7[a]	H	H, iPr	**Ir7**
L8[a]	H	iPr, H	**Ir8**
L9[a]	H	H, Ph	**Ir9**
L10[a]	H	Ph, H	**Ir10**

Scheme 1 Synthetic route used to access the (phox) ligands **L1-10** and the corresponding half-sandwich iridium chlorido complexes **Ir1-10**, chlorido ligand exchange in DMSO. [a]Procedure **A.** a) CH_2Cl_2, r.t.; b) $SOCl_2$ (4 eq), CH_2Cl_2, r.t. [b]Procedure **B.** a) CH_2Cl_2, r.t.; b) $SOCl_2$ (4 eq), CH_2Cl_2, r.t. ; c) NaH (1 eq), THF, r.t. Procedure **C.** NaOAc (6 eq), CH_2Cl_2, r.t.

Fig. 1 Molecular structure of **Ir1** determined by X-ray crystallography with thermal ellipsoids drawn at 50% probability. The hydrogen atoms have been omitted for clarity. Selected bond lengths (Å): Ir-Cl 2.4084(9), Ir-N 2.076(3), Ir-C 2.054(3), C-Ir-N 77.89(13).

The phenyl group coordinates the iridium atom from a C-H bond activation reaction which rate was proven to depend on the electronic nature of the ligand.[18] The oxazoline's hydrogens in the ^{1}H NMR spectra of all the complexes were magnetically inequivalent owing to the chiral environment around the iridium atom.

Owing to the presence of another stereogenic centre on chiral ligands **L7-10**, complexes **Ir7** to **Ir10**, were obtained as mixtures of diastereomers. **Ir7-8** were obtained in a 9:1 diastereomeric ratio[18] whereas **Ir9-10** were obtained in a 1:1 ratio measured by ^{1}H NMR in DMSO-d_6. However, a coordinating environment like DMSO-d_6 induces epimerization of the (phox)-chelated complexes at the iridium centre and the diastereomeric excess quantification is no longer relevant. The molecular structure of **Ir1** solved by X-ray diffraction analysis (Fig. 1, Tables S1-2) showed the expected "piano stool" geometry typical of this family of complexes.

Reactivity towards the DMSO vehicle

DMSO is a widely used administration solvent for metal complexes owing to its ability to solubilise highly lipophilic structures and its convenient miscibility with water. Despite its relatively low toxicity, DMSO has been shown to exert a negative effect on the activation process of cisplatin (CDDP)[19] and a rapid formation of a solvento adduct was reported for ruthenium half-sandwich complexes.[20]

The vehicle used for further biological tests being DMSO, the stability of the complexes in this solvent was investigated by ^{1}H NMR spectroscopy. The characteristic chemical shift of the Cp* ligand was used to monitor the conversion of **Ir1-10** to [Ir-DMSO-d_6]$^+$ (Fig. S1). At 297K, most complexes undergo a very fast chlorido to DMSO ligand exchange with half-lives below 12 min (**Ir1**, **Ir2**, **Ir4**, **Ir6**, **Ir9-10**) albeit with an electronic effect observed for **Ir3** and **Ir5** that is linked to the σ-I Hammett constant of fluoro and nitro substituents. **Ir5**'s half-life in DMSO-d_6 was the longest of the series, that is 270 min thus 20-fold longer than that of **Ir3** (Table S3).

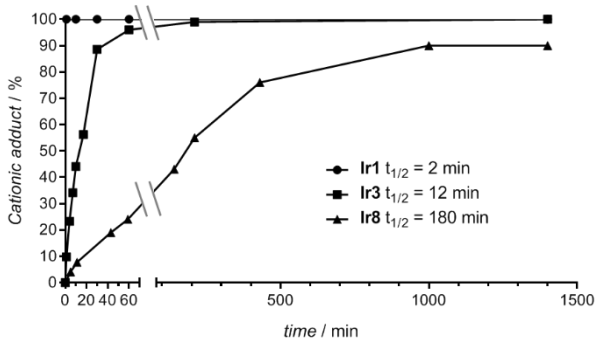

Fig. 2 Comparison of the rates of solvolysis of three representative complexes in DMSO-d_6. Quantification was done by integration of the characteristic ^{1}H NMR peak of the Cp* ligand of the two forms (Fig. S1). Half-lives of **Ir1-10** are presented in Table S3.

For comparison, the half-sandwich iridium complex carrying the 2-phenylpyridine ligand showed a much lower rate of

exchange with a half-life of 1125 min.[21] This structure-based approach demonstrates that the Ir-Cl bond strength is correlated to the electron-withdrawing character of the substituent on the (phox) ligand. Furthermore, the steric effect induced by the substitutions $R^{2,3}$ on the oxazoline ring is another parameter affecting the exchange rate since **Ir7-8** also present an extended half-life. At equilibrium, the ligand exchange is total for most complexes of the series except for **Ir2** and **Ir7-8** for which the establishment of a (1:9) ratio was observed between the neutral and cationic forms (Fig. 2).

To check whether the DMSO adducts could further undergo aquation once diluted in the cell-culture medium, a [**Ir1**-DMSO]$^+$ complex was synthesized and isolated as a nitrate salt (see procedure in Fig. S2). Its ^{1}H NMR spectrum in CD_3OD/D_2O (2:1) showed that no water/DMSO exchange took place. On the other hand, addition of a saturating amount of NaCl (1.1 M) resulted in the coalescence of the two singlets around 2.89 ppm attributed to two methyl groups, marking a very fast exchange between DMSO and Cl^- at the NMR timescale. The high chloride concentration also favoured the partial displacement of DMSO by Cl^- affording a mixture of cationic and neutral complexes in 9:1 ratio at equilibrium. This experiment proved the stability of the DMSO adduct, ruling out the formation of an aqua complex and supported the hypothesis that the cationic DMSO complexes are the true administered molecules in the biological assays.

The ability of **Ir2** to undergo aquation was also examined by ^{1}H NMR in MeOD-d_4 / D_2O (3:2). Addition of D_2O caused peak broadening but the chemical shift of all the protons remained the same. Further addition of NaCl restored the initial peaks width (Fig. S3). Therefore, no hydrolysis of the Ir-Cl bond of **Ir2** took place in these conditions.

Cytotoxicity assays

The library of iridium complexes was examined for toxicity. Prior to cell assays, stock solutions of **Ir1-10** in DMSO were incubated at room temperature for 24 h to ensure that the equilibrium between the neutral and the cationic forms was reached for each complex. Their IC_{50} on the HeLa cancer cell line were evaluated using the MTT cell viability assay. The obtained values are comprised between 3 and 6 µM (Table 1), in good agreement with values previously on the same cell line for half-sandwich iridium complexes bearing anionic C^O chelating ligands.[22] This rather narrow range depicts the minor influence of the substituents carried by the chelating ligand on the antiproliferative activity as well as the stereochemistry of the phox ligand. This result dramatically contrasts with previous reports on structurally related complexes for which the substitution pattern greatly influenced the IC_{50} values.[23–25]

The cell response to **Ir2**, **Ir4**, **Ir8** and **Ir10** was also investigated by a complementary label-free viability assay based on impedance readout, using the xCELLigence Real Time Cell Analysis (RTCA) system that allows the dynamic monitoring of live cell adhesion and proliferation. All compounds induced a dose-dependent and immediate loss of cell adhesion. As illustrated in Fig. S4 for **Ir8**, cells treated at concentrations close to the IC_{50} were able to re-adhere and then to proliferate although at lower rates, as a consequence of either inhibition of cell division or cell death or both (see videomicroscopy SI). The resulting time-dependent IC_{50} was found to reach a minimum after 48 h of treatment and **Ir8** was the most active compound of the series with an IC_{50} of 3.6 µM (Table 1).

Compound	MTT IC_{50} (µM)[a]	RTCA IC_{50} (µM)[b]
Ir1	4.17 ± 0.11	ND[c]
Ir2	4.05 ± 0.47	5.06 ± 0.23
Ir3	3.56 ± 0.68	ND
Ir4	3.73 ± 0.99	4.72 ± 0.82
Ir5	4.47 ± 0.29	ND
Ir6	5.81 ± 0.61	ND
Ir7	3.46 ± 0.29	ND
Ir8	3.06 ± 0.38	3.59 ± 0.15
Ir9	3.35 ± 0.24	ND
Ir10	3.36 ± 0.57	4.41 ± 0.59

Table 1 Antiproliferative activity of **Ir1-10** towards the HeLa cell line

[a] Median inhibiting concentration after 96 h of treatment assessed by the MTT cell viability assay. [b] Median inhibiting concentration after 48 h of treatment assessed by the xCELLigence RTCA system. [c] Not determined.

Apoptosis assay

Morphological changes induced by **Ir1-10** were suggestive of regulated cell death. Apoptosis is characterised by hierarchical activation of caspases by proteolytic processing, with the effector caspase-3 being a critical executioner that degrades many cellular proteins. We thus used caspase-3 cleavage as a readout of apoptosis in treated samples. Fig. 3 shows the presence of cleaved caspase-3 in iridium-treated samples starting 12 h after drug administration, a fast kinetics compared to conditions of etoposide-induced DNA damage suggesting a different MoA. Overall these results point to regulated cell death induced by the complexes regardless of their substitution pattern.

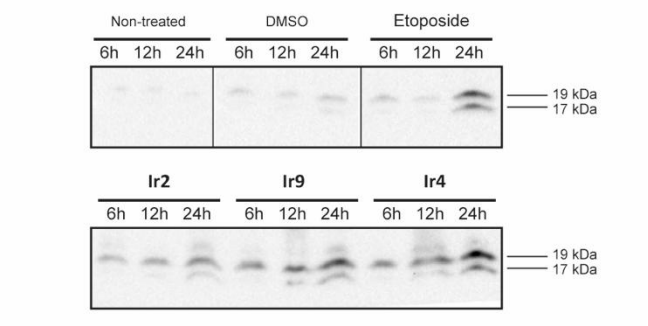

Fig. 3 Immunoblot showing accumulation of cleaved caspase-3 fragments at 19 and 17 kDa for the indicated time (h) after addition of 10 µM compound or vehicle (DMSO). Three representative complexes of the series are presented. Etoposide, a clinically approved topoisomerase II inhibitor that induces single and double strand DNA breaks, was used as positive control and showed the presence of the cleaved form of caspase-3 after 24 h. Equal loadings were assessed by Ponceau S staining (Fig. S5).

In vitro catalytic activity

The reaction of various half-sandwich iridium complexes with NADH is widely described in the literature.[26] Some structures are able to form metal hydride complexes with concomitant formation of NAD^+ following a dissociative mechanism according to DFT calculation[27]. Hydride can then be transferred to various acceptors such as flavin mononucleotide (FMN),[28] pyruvate to form lactate,[29] proton to form dihydrogen,[30] aldehydes to form alcohols[31,32] or imines to yield amines.[33] It was also shown that dioxygen could act as hydride acceptor to yield hydrogen peroxide which presence after 48 h incubation of NADH and complexes in aerated solutions was qualitatively detected using a peroxides test stick.[12,34]

The ability of **Ir1-10** to catalyse NADH oxidation was firstly investigated by monitoring the absorbance at 340 nm of a 100 µM solution of NADH in 5 mM phosphate buffer/MeOH (99:1) in the presence of 10 mol% complex during 150 min. Reactions were performed with stock solutions of chlorido complexes in MeOH as we found that the Ir-DMSO adduct was less active (Fig. S7), which is consistent with the poor lability of the DMSO ligand (Fig. S2). As NADH oxidation was previously shown to generate various side-products,[35] results are expressed in concentration of remaining substrate after 150 min (Fig. 4). All the complexes catalysed the oxidation of NADH. Moreover, the moderately contrasted data show again a modest influence of the ligand substitution pattern on this process. Resulting TONs at 2.5 h were calculated for **Ir1-10** (Table S4) and all values are higher than 1, confirming the catalytic nature of this reaction.

Secondly, we examined whether oxidation of NADH was accompanied by the production of H_2O_2 in the presence of O_2, the iridium complexes thus mimicking NADH oxidase activity (See catalytic pathway in Fig. S8). For this, the production of H_2O_2 was monitored for the first time using the HRP-linked Amplex Red® assay over 150 min. Since NADH autooxidation is known to give false positive results in this assay, we added 40 U/mL of SOD to prevent the formation of radical intermediates that spontaneously oxidize the Amplex substrate, following recommendations from the literature.[36] Although all of the complexes were able to accept a hydride from coenzyme NADH, only the oxazoline-substituted complexes (**Ir2**, **Ir7-10**) were able to transfer their hydride to dissolved O_2, producing detectable amounts of hydrogen peroxide (Fig. 4). This trend may be due to differences of hydricity, i.e. hydride donor strength, among the complexes[37] which may be linked to the electron-donating property of the alkyl / aryl substituent on the oxazoline ring of the chelating ligand. Reassuringly, the couples of isomers (**Ir7-8** and **Ir9-10**) displayed a similar potency to catalyse the production of H_2O_2. These four complexes along with **Ir2** display the highest potency towards this overall process, showing that the hydride transfer to form H_2O_2 is mainly dependent on steric hindrance around the labile position.

Intracellular H_2O_2 production

Among cellular reactive oxygen species (ROS), hydrogen peroxide is involved in various metabolic pathways and is suspected of having a signalling role in natural biological processes.[38] According to the literature, iridium half-sandwich complexes including 2-phenylpyridine as chelating ligand were shown to induce oxidative stress (i.e. total ROS and RNS levels increase) in cancer cells and this was suggested to result from the catalytic production of H_2O_2.[12] We thus investigated whether the ability of **Ir1-10** to catalyse the production of H_2O_2 *in vitro* could be correlated to their cytotoxicity and their capacity to elevate intracellular H_2O_2.

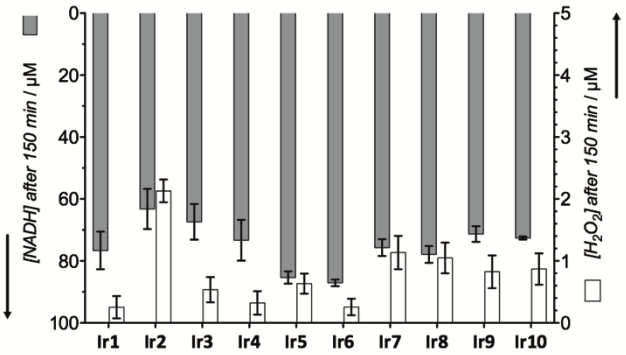

Fig. 4 Amounts of remaining NADH and H_2O_2 produced in model physiological environment. Data are shown as mean ± SD of three experiments performed at 37°C in 5 mM phosphate buffer pH 7.4 containing 1% MeOH in the presence of 10 mol% iridium complex. Hydrogen peroxide was quantified using a multiplex measurement of triplicates and standard for each experiment.

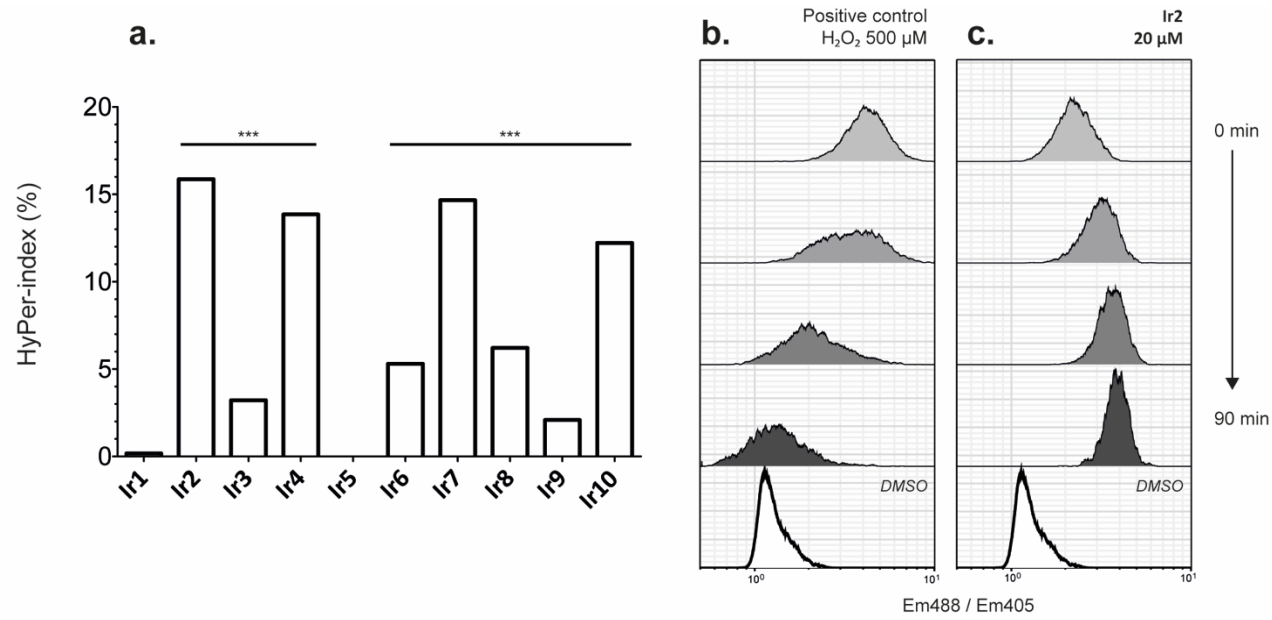

Fig. 5 **a.** HyPer index derived from the median values of HeLa cells exposed to 10 µM **Ir1-10** for 60 min (at least 5 000 gated events). Statistical significance was compared to the negative control with a Mann-Whitney non-parametric t-test ($p < 0.0001$) **b.** Evolution of the HyPer ratios over time after addition of a saturating amount of hydrogen peroxide. **c.** Evolution of the HyPer ratios over time after addition of 20 µM **Ir2**, similar results were obtained with lower concentrations and are reported in Fig. S6. Cells treated for 90 min with DMSO were used as negative control.

Instead of employing classical but non-selective chemical ROS probes such as H_2DCFDA, we used a fluorescent protein-based H_2O_2-selective redox sensor, the HyPer ratiometric probe developed by Belousov et al.[39] The spectral properties of the HyPer sensor change upon its reversible oxidation by H_2O_2 and reduction by glutathione-dependent reductases, thus allowing the indirect measurement of intracellular H_2O_2.

A stable HeLa cell line that constitutively expresses HyPer[40] was exposed to **Ir1-10**, then reduced and oxidized forms of HyPer were quantified by flow cytometry as the ratio of fluorescence emission at 520 nm after excitation at 405 and 488 nm respectively (Fig. S6).

The median ratios M of the HyPer-expressing cells were used to calculate a HyPer-index[41] H which was quantified in % according to Equation (1) :

$$H = \frac{(M - M_{DMSO})}{(M_{H_2O_2} - M_{DMSO})} \qquad (1)$$

where M_{DMSO} and $M_{H_2O_2}$ correspond to the median ratio values obtained for the negative and positive controls, respectively. This index directly shows the significance of the observed variations upon a 60-min treatment with 10 µM **Ir1-10** (Fig. 5a). Dramatic differences between the complexes were immediately observed with **Ir2**, **Ir4**, **Ir7** and **Ir10** displaying high HyPer indexes while **Ir1** and **Ir5** were fully unable to induce H_2O_2 production in HeLa cells. Since **Ir2** complex displayed the highest HyPer index, the rate of this increase was also monitored over a time course of 80 min. As a positive control, cells exposed to a saturating amount of hydrogen peroxide (Fig. 5b, Fig. S6) exhibited a fast recovery with the ratiometric median parameter decreasing to a basal value within an hour, as a result of cellular detoxification processes. In contrast upon treatment with **Ir2** in the same time lapse (Fig. 5c), H_2O_2 levels rose progressively suggesting an uncompensated production of H_2O_2 that is presumably catalytic. Moreover, the rate of H_2O_2 production was also concentration-dependent in the 5 – 20 µM range (Fig. S6).

Conclusions

In summary, we have reported the synthesis and characterization of a set of half-sandwich iridium complexes comprising a phenyloxazoline chelating ligand with a wide range of substituents. We examined their outcome in the vehicle and the stability of the resulting DMSO adducts in the presence of water. These adducts are cationic, more lipophilic and thus susceptible to display an enhanced penetration across cellular membranes. The strong coordinating power of DMSO to iridium suggests that the lifetimes of the cationic iridium complexes may be long in the intracellular context. Altogether, it appears necessary to properly determine the stability of the drug in the vehicle, a feature scarcely described in the literature, since it can dramatically influence its biological activity. This study also highlighted the minor influence of the structural modifications of the (phox) ligand on the overall toxicity of the complexes, all of them inducing cell death by apoptosis. *In vitro*, all complexes were able to accept a hydride from coenzyme NADH, but they were not equally able to transfer it to dioxygen to produce H_2O_2. We quantified for the first time the production of hydrogen peroxide elicited by half-sandwich iridium complexes in two experimental settings, both *in vitro* and *in vivo*. We found that the complexes carrying substituents on the oxazoline ring (**Ir2**, **Ir7-10**) were the most efficient catalysts of H_2O_2 production *in*

vitro. Strikingly, among these molecules, **Ir2**, **Ir7** and **Ir10** were also proven to generate high levels of H_2O_2 in living cells during the first hour of treatment. Moreover, the cells' detoxification machinery was not able to compensate this production over time unlike with a simple hydrogen peroxide addition. While this mode of action provides a rationale for the fast cytotoxicity of the compounds that induced intracellular accumulation of H_2O_2, it cannot be excluded that other mechanisms be at stake, leading to the fast activation of caspase-3 and cell death by apoptosis. Indeed, neither **Ir1** nor **Ir5** were efficient in both analyses despite a comparable antiproliferative activity. Recent studies have shown that a structurally related iridium complex exhibited a mitochondrial tropism and induced distortions of the inner membrane.[42] A future challenge will be to decipher whether this accumulation of H_2O_2 results from mitochondrial disruption or is a direct consequence of intracellular transfer hydrogenation catalysed by the iridium complexes.

Conflicts of interest

There are no conflicts to declare.

Acknowledgements

This research was supported by the IPV doctoral program of Sorbonne Université. We wish to acknowledge basic support from CNRS, INSERM and Sorbonne Université, to UMR_8232 and UMR_S938 and competitive funding from LabEx MiChem part of French state funds managed by the ANR within the Investissements d'avenir programme under reference ANR-11-IDEX-004-02 and from INCA-DGOS-Inserm_12560 SiRIC CURAMUS financially supported by the French National Cancer Institute, the French Ministry of Solidarity and Health and Inserm. We thank Dr. Sophie Vriz for the gift of HeLa-HyPer stable cell line. We are indebted to Blaise Gatin-Fraudet and Kévin Passador for supporting technical assistance and data acquisition and to Romain Morichon for videomicroscopy experiments.

References

1 L. Zeng, P. Gupta, Y. Chen, E. Wang, L. Ji, H. Chao and Z.-S. Chen, The development of anticancer ruthenium(II) complexes: from single molecule compounds to nanomaterials, *Chem. Soc. Rev.*, 2017, **46**, 5771–5804.

2 C. Caporale and M. Massi, Cyclometalated iridium(III) complexes for life science, *Coord. Chem. Rev.*, 2018, **363**, 71–91.

3 P. Zhang, H. Huang, S. Banerjee, G. J. Clarkson, C. Ge, C. Imberti and P. J. Sadler, Nucleus-Targeted Organoiridium-Albumin Conjugate for Photodynamic Cancer Therapy, *Angew. Chem. Int. Ed.*, 2019, **58**, 2350–2354.

4 X. Li, W. Ouyang, J. Nie, S. Ji, Q. Chen and Y. Huo, Recent Development on Cp*Ir(III)-Catalyzed C−H Bond Functionalization, *ChemCatChem*, 2020, **12**, 2358–2384.

5 C. Michon, K. MacIntyre, Y. Corre and F. Agbossou-Niedercorn, Pentamethylcyclopentadienyl Iridium(III) Metallacycles Applied to Homogeneous Catalysis for Fine Chemical Synthesis, *ChemCatChem*, 2016, **8**, 1755–1762.

6 J. Liu, X. Wu, J. A. Iggo and J. Xiao, Half-sandwich iridium complexes—Synthesis and applications in catalysis, *Coord. Chem. Rev.*, 2008, **252**, 782–809.

7 Z. Liu, L. Salassa, A. Habtemariam, A. M. Pizarro, G. J. Clarkson and P. J. Sadler, Contrasting Reactivity and Cancer Cell Cytotoxicity of Isoelectronic Organometallic Iridium(III) Complexes, *Inorg. Chem.*, 2011, **50**, 5777–5783.

8 R. M. Lord and P. C. McGowan, Organometallic Iridium Arene Compounds: The Effects of *C* -Donor Ligands on Anticancer Activity, *Chem. Lett.*, 2019, **48**, 916–924.

9 Y. Yang, X. Ge, L. Guo, T. Zhu, Z. Tian, H. Zhang, Q. Du, H. Peng, W. Ma and Z. Liu, Zwitterionic and cationic half-sandwich iridium(III) ruthenium(II) complexes bearing sulfonate groups: synthesis, characterization and their different biological activities, *Dalton Trans.*, 2019, **48**, 3193–3197.

10 J. M. Zimbron, K. Passador, B. Gatin-Fraudet, C.-M. Bachelet, D. Plażuk, L.-M. Chamoreau, C. Botuha, S. Thorimbert and M. Salmain, Synthesis, Photophysical Properties, and Living Cell Imaging of Theranostic Half-Sandwich Iridium–4,4-Difluoro-4-bora-3 *a* ,4 *a* -diaza- *s* -indacene (BODIPY) Dyads, *Organometallics*, 2017, **36**, 3435–3442.

11 Z. Liu, I. Romero-Canelón, A. Habtemariam, G. J. Clarkson and P. J. Sadler, Potent Half-Sandwich Iridium(III) Anticancer Complexes Containing C^N-Chelated and Pyridine Ligands, *Organometallics*, 2014, **33**, 5324–5333.

12 Z. Liu, I. Romero-Canelón, B. Qamar, J. M. Hearn, A. Habtemariam, N. P. E. Barry, A. M. Pizarro, G. J. Clarkson and P. J. Sadler, The Potent Oxidant Anticancer Activity of Organoiridium Catalysts, *Angew. Chem. Int. Ed.*, 2014, **53**, 3941–3946.

13 J. M. Hearn, G. M. Hughes, I. Romero-Canelón, A. F. Munro, B. Rubio-Ruiz, Z. Liu, N. O. Carragher and P. J. Sadler, Pharmaco-genomic investigations of organo-iridium anticancer complexes reveal novel mechanism of action, *Metallomics*, 2018, **10**, 93–107.

14 D. Trachootham, J. Alexandre and P. Huang, Targeting cancer cells by ROS-mediated mechanisms: a radical therapeutic approach?, *Nat. Rev. Drug Discov.*, 2009, **8**, 579–591.

15 C. Gorrini, I. S. Harris and T. W. Mak, Modulation of oxidative stress as an anticancer strategy, *Nat. Rev. Drug Discov.*, 2013, **12**, 931–947.

16 J. H. Barnard, C. Wang, N. G. Berry and J. Xiao, Long-range metal–ligand bifunctional catalysis: cyclometallated iridium catalysts for the mild and rapid dehydrogenation of formic acid, *Chem. Sci.*, 2013, **4**, 1234.

17 D. L. Davies, O. Al-Duaij, J. Fawcett, M. Giardiello, S. T. Hilton and D. R. Russell, Room-temperature cyclometallation of amines, imines and oxazolines with $[MCl_2Cp^*]_2$ (M = Rh, Ir) and $[RuCl_2(p\text{-cymene})]_2$, *Dalton Trans*, 2003, 4132–4138.

18 Y. Boutadla, D. L. Davies, R. C. Jones and K. Singh, The Scope of Ambiphilic Acetate-Assisted Cyclometallation with Half-Sandwich Complexes of Iridium, Rhodium and Ruthenium, *Chem. - Eur. J.*, 2011, **17**, 3438–3448.

19 M. D. Hall, K. A. Telma, K.-E. Chang, T. D. Lee, J. P. Madigan, J. R. Lloyd, I. S. Goldlust, J. D. Hoeschele and M. M. Gottesman, Say No to DMSO: Dimethylsulfoxide Inactivates Cisplatin, Carboplatin, and Other Platinum Complexes, *Cancer Res.*, 2014, **74**, 3913–3922.

20 M. Patra, T. Joshi, V. Pierroz, K. Ingram, M. Kaiser, S. Ferrari, B. Spingler, J. Keiser and G. Gasser, DMSO-Mediated Ligand Dissociation: Renaissance for Biological Activity of *N* -

Heterocyclic-[Ru(η ^{6} -arene)Cl $_{2}$] Drug Candidates, *Chem. - Eur. J.*, 2013, **19**, 14768–14772.
21 A. C. Carrasco, V. Rodríguez-Fanjul, A. Habtemariam and A. M. Pizarro, Structurally Strained Half-Sandwich Iridium(III) Complexes As Highly Potent Anticancer Agents, *J. Med. Chem.*, 2020, **63**, 4005–4021.
22 Q. Du, L. Guo, M. Tian, X. Ge, Y. Yang, X. Jian, Z. Xu, Z. Tian and Z. Liu, Potent Half-Sandwich Iridium(III) and Ruthenium(II) Anticancer Complexes Containing a P^O-Chelated Ligand, *Organometallics*, 2018, **37**, 2880–2889.
23 J. Yellol, S. A. Pérez, A. Buceta, G. Yellol, A. Donaire, P. Szumlas, P. J. Bednarski, G. Makhloufi, C. Janiak, A. Espinosa and J. Ruiz, Novel C,N-Cyclometalated Benzimidazole Ruthenium(II) and Iridium(III) Complexes as Antitumor and Antiangiogenic Agents: A Structure–Activity Relationship Study, *J. Med. Chem.*, 2015, **58**, 7310–7327.
24 Y. Yang, L. Guo, Z. Tian, Y. Gong, H. Zheng, S. Zhang, Z. Xu, X. Ge and Z. Liu, Novel and Versatile Imine-N-Heterocyclic Carbene Half-Sandwich Iridium(III) Complexes as Lysosome-Targeted Anticancer Agents, *Inorg. Chem.*, 2018, **57**, 11087–11098.
25 A. J. Millett, A. Habtemariam, I. Romero-Canelón, G. J. Clarkson and P. J. Sadler, Contrasting Anticancer Activity of Half-Sandwich Iridium(III) Complexes Bearing Functionally Diverse 2-Phenylpyridine Ligands, *Organometallics*, 2015, **34**, 2683–2694.
26 Y. Okamoto and T. R. Ward, Transfer Hydrogenation Catalyzed by Organometallic Complexes Using NADH as a Reductant in a Biochemical Context, *Biochemistry*, 2017, **56**, 5223–5224.
27 I. Ritacco, N. Russo and E. Sicilia, DFT Investigation of the Mechanism of Action of Organoiridium(III) Complexes As Anticancer Agents, *Inorg. Chem.*, 2015, **54**, 10801–10810.
28 S. Shibata, T. Suenobu and S. Fukuzumi, Direct Synthesis of Hydrogen Peroxide from Hydrogen and Oxygen by Using a Water-Soluble Iridium Complex and Flavin Mononucleotide, *Angew. Chem. Int. Ed.*, 2013, **52**, 12327–12331.
29 S. Betanzos-Lara, Z. Liu, A. Habtemariam, A. M. Pizarro, B. Qamar and P. J. Sadler, Organometallic Ruthenium and Iridium Transfer-Hydrogenation Catalysts Using Coenzyme NADH as a Cofactor, *Angew. Chem. Int. Ed.*, 2012, **51**, 3897–3900.
30 Y. Maenaka, T. Suenobu and S. Fukuzumi, Efficient Catalytic Interconversion between NADH and NAD $^{+}$ Accompanied by Generation and Consumption of Hydrogen with a Water-Soluble Iridium Complex at Ambient Pressure and Temperature, *J. Am. Chem. Soc.*, 2012, **134**, 367–374.
31 A. H. Ngo, M. Ibañez and L. H. Do, Catalytic Hydrogenation of Cytotoxic Aldehydes Using Nicotinamide Adenine Dinucleotide (NADH) in Cell Growth Media, *ACS Catal.*, 2016, **6**, 2637–2641.
32 S. Bose, A. H. Ngo and L. H. Do, Intracellular Transfer Hydrogenation Mediated by Unprotected Organoiridium Catalysts, *J. Am. Chem. Soc.*, 2017, **139**, 8792–8795.
33 M. Soetens, F. Drouet and O. Riant, (η ^{5} -Pentamethylcyclopentadienyl)iridium Complex Catalyzed Imine Reductions Utilizing the Biomimetic 1,4-NAD(P)H Cofactor and *N* -Benzyl-1,4-dihydronicotinamide as the Hydride-Transfer Agent, *ChemCatChem*, 2017, **9**, 929–933.
34 Z. Liu and P. J. Sadler, Formation of glutathione sulfenate and sulfinate complexes by an organoiridium(III) anticancer complex, *Inorg Chem Front*, 2014, **1**, 668–672.
35 A. Bucci, S. Dunn, G. Bellachioma, G. Menendez Rodriguez, C. Zuccaccia, C. Nervi and A. Macchioni, A Single Organoiridium Complex Generating Highly Active Catalysts for both Water Oxidation and NAD $^{+}$ /NADH Transformations, *ACS Catal.*, 2017, **7**, 7788–7796.
36 T. V. Votyakova and I. J. Reynolds, Detection of hydrogen peroxide with Amplex Red: interference by NADH and reduced glutathione auto-oxidation, *Arch. Biochem. Biophys.*, 2004, **431**, 138–144.
37 A. H. Ngo and L. H. Do, Structure–activity relationship study of half-sandwich metal complexes in aqueous transfer hydrogenation catalysis, *Inorg. Chem. Front.*, 2020, **7**, 583–591.
38 C. Rampon, M. Volovitch, A. Joliot and S. Vriz, Hydrogen Peroxide and Redox Regulation of Developments, *Antioxidants*, 2018, **7**, 159.
39 D. S. Bilan and V. V. Belousov, HyPer Family Probes: State of the Art, *Antioxid. Redox Signal.*, 2016, **24**, 731–751.
40 C. Gauron, F. Meda, E. Dupont, S. Albadri, N. Quenech'Du, E. Ipendey, M. Volovitch, F. Del Bene, A. Joliot, C. Rampon and S. Vriz, Hydrogen peroxide (H 2 O 2) controls axon pathfinding during zebrafish development, *Dev. Biol.*, 2016, **414**, 133–141.
41 O. G. Lyublinskaya, Ju. S. Ivanova, N. A. Pugovkina, I. V. Kozhukharova, Z. V. Kovaleva, A. N. Shatrova, N. D. Aksenov, V. V. Zenin, Yu. A. Kaulin, I. A. Gamaley and N. N. Nikolsky, Redox environment in stem and differentiated cells: A quantitative approach, *Redox Biol.*, 2017, **12**, 758–769.
42 J. J. Conesa, A. C. Carrasco, V. Rodríguez-Fanjul, Y. Yang, J. L. Carrascosa, P. Cloetens, E. Pereiro and A. M. Pizarro, Unambiguous Intracellular Localization and Quantification of a Potent Iridium Anticancer Compound by Correlative 3D Cryo X-Ray Imaging, *Angew. Chem. Int. Ed.*, 2020, **59**, 1270–1278.